DEVELOPMENT OF A TERRESTRIAL AEROSOL MEASUREMENTS USING DIGITAL CAMERAS

WONG CHOW JENG

UNIVERSITI SAINS MALAYSIA

2016

DEVELOPMENT OF A TERRESTRIAL AEROSOL MEASUREMENTS USING DIGITAL CAMERAS

by

WONG CHOW JENG

Thesis submitted in fulfilment of the requirements
for the degree of
Doctor of Philosophy

September 2016

ACKNOWLEDGEMENT

I would like to express my sincere gratitude to my supervisor Professor Mohd. Zubir Mat Jafri and co-supervisors Associate Professors Khiruddin Abdullah and Associate Professors Lim Hwee San. They provided me with the advice and feedback throughout the preparation of this thesis. I gratefully acknowledge Universiti Sains Malaysia and School of Physics, for its permission to use facilities for this research work. This research was funded by e-science Fund 01-01-05-SF0139 from the Ministry of Science, Technology and Innovation, Malaysia and Short Term Grant from Universiti Sains Malaysia. My parents deserve very special thanks for their persistent support, understanding and encouragement throughout my life. I want to thank my family. The encouragement and support from my beloved wife and our always positive and joyful children is a powerful source of inspiration and energy. Finally, and most importantly, I would like to thank the almighty God, for it is under his grace that we live, learn and flourish.

TABLE OF CONTENTS

ACKNOWLEDGEMENT ii

TABLE OF CONTENTS iii

LIST OF TABLES vi

LIST OF FIGURES vii

LIST OF SYMBOLS xi

LIST OF ABBREVIATIONS xii

ABSTRAK xiii

ABSTRACT xv

CHAPTER 1 : INTRODUCTION

1.1 Background 1

1.2 Problem Statement 7

1.3 Aim 8

1.4 Objectives 8

1.5 Novelty and Significance 9

1.6 Scope 9

1.7 Thesis overview 11

CHAPTER 2 : LITERATURE REVIEW

2.1 Measurement of atmospheric aerosols 13

2.2 Atmospheric aerosols 17

2.2.1 Size and behaviour of atmospheric aerosols 17

2.2.2 The level of air pollution for atmospheric aerosols 19

2.3 Visibility related atmospheric aerosols concentration 22

2.4 Theoretical derivation of algorithm 23

CHAPTER 3 : METHODOLOGY

3.1 Location of study 30

3.2 Digital camera selection 30

3.3 Digital camera setting for landscape photography 33

3.3.1 Digital SLR camera setting 33

3.3.2 Consumer compact digital camera setting 35

3.3.3 Video digital camera setting 36

3.3.4 Photograph noise reduction setting 37

3.4 Camera calibration 38

3.4.1 Determination of spectral sensitivity and spectral bands of the digital camera sensors 38

3.4.2 Determination of the relationship between the irradiance and the digital numbers of images 43

3.4 Development of atmospheric aerosols concentration algorithm 46

3.5 Measuring the atmospheric concentration by using digital cameras 51

3.6 Validating the atmospheric aerosols concentration measured by using digital cameras 53

CHAPTER 4 : RESULTS AND DISCUSSION

4.1 Calibration of the Digital Cameras 54

4.1.1 Determination of the Spectral Sensitivity and Spectral Bands of the Sensors for Digital Cameras 54

4.1.2 Calibration of the Sensors for Digital Cameras 66

4.2 Developing Algorithm 73

4.2.1 Determination of Reflectance of Target Reference Surface 73

4.2.2 Determination of Irradiance Recorded by Digital Camera 76

4.2.3 Determination of the Irradiance of Diffused Sunlight from the Sky 78
4.2.4 Determination of Reflectance Recorded by Digital Camera Sensors 80
4.2.5 Determination of Reflectance from Atmospheric Aerosols 82
4.2.6 Determination of the Relationship between the Aerosol Concentration of PM10 and the Reflectance from Atmospheric Aerosols 83
4.3 Measuring Atmospheric Aerosols Concentration Using Digital Cameras 86
4.3.1 Measurement of Atmospheric Aerosols Concentration Using Five Different Digital Cameras 86
4.3.2 Measurement of Different Atmospheric Aerosols Concentration Using a Single Digital Cameras 90
4.4 Validating the Measurements of Atmospheric Aerosol Concentration using Digital Cameras 93

CHAPTER 5 : CONCLUSION AND FUTURE WORK

5.1 Conclusion 97
5.2 Future Work 98

REFERENCES 100

APPENDICES

Appendix A Atmospheric Radiative Transfer 107
Appendix B Cameras specification 113
Appendix C MATLAB Programming (Crop image to obtain average digital number for RGB) 119
Appendix D DustTrak™ specification 121
Appendix E Calibration certificate for DustTrak Meter 122
Appendix F Data 123

PUBLICATION LIST 127

LIST OF TABLES

		Page
Table 2.1	The official Health Implications of the respective Air Pollution Index (API) in Malaysia. (From Department of Environment, Ministry of Natural Resources and Environment, Malaysia)	21
Table 3.1	Specification of the respective cameras used in this study	32
Table 3.2	Digital SLR camera setting for landscape photography	34
Table 4.1	A list of H-20 monochromator set wavelengths of monochromatic light with its corresponding wavelengths λ_{eff} and uncertainty	57
Table 4.2	Table of the RGB spectral bands for the five digital cameras used in this study	66
Table 4.3	The RGB average digital numbers, DN (Canon 400D digital camera) and the isolated RGB spectral irradiance, L of the color filtered light	69
Table 4.4	Regression analysis results for the data of the isolated RGB spectral irradiance, L and the RGB average digital numbers, DN for the five digital cameras used. (Canon 400D digital camera, Nikon D200 digital camera, Canon IXUS 40 digital camera, BOSCH Auto Dome 300 Series Surveillance Camera, and Logitech QuickCam 4000 Webcam.)	71
Table 4.5	A summary of the green vegetation reflectance from the target reference surface for the RGB bands captured by Canon 400D DSLR camera, Nikon D200 DSLR camera, Canon IXUS 40 digital camera, BOSCH Auto Dome 300 Series Surveillance Camera, and Logitech QuickCam 4000 Webcam	76
Table 4.6	The spectral irradiance of diffused sunlight from the sky which was isolated according to the RGB spectral bands of the Canon 400D DSLR camera at different times of the day on 15 May 2015	79
Table 4.7	The results of regression analysis for the atmospheric aerosols concentration data and the data of reflectance from atmospheric aerosols recorded by the Canon 400D DSLR camera	84
Table 4.8	A summary of the selected algorithms to determine the atmospheric aerosols concentration using Canon 400D DSLR camera, Nikon D200 DSLR camera, Canon IXUS 40 digital camera, BOSCH Auto Dome 300 Series Surveillance Camera, and Logitech QuickCam 4000 Webcam	85
Table 4.9	A comparison of the DustTrak meter readings and the atmospheric aerosols concentration, PM10 determined by the Canon 400D DSLR camera.	92

LIST OF FIGURES

		Page
Figure 1.1	Air pollutants being released from the Sultan Azlan Shah Coal Power Station in Manjung, Perak, Malaysia. (Tenaga Nasional Berhad, 2014).	1
Figure 1.2	The annual average benchmarking data of the air quality for PM_{10}, SO_2, and NO_2 concentrations in twenty two selected Asian cities. (Asian Green City Index, 2014)	3
Figure 1.3	Images of Scanning Electron Microscope (SEM) for soot particles of air pollutants from a coal-fired power plant. Magnification: (a) 500X, (b) 1,500X, (c) 2,000X and (d) 2,500X (Cheng, 1979)	4
Figure 2.1	An illustration of the definition of aerodynamic diameter, D_a for two particles of different shapes (Hinds, 1999)..	18
Figure 2.2	The aerial perspective model to show the digital camera recording the lights propagated through atmospheric the pollutant column. These lights are from reflected light of target reference surface, R_T and reflected light of atmospheric aerosols, R_{Atm}	24
Figure 3.1	Aerial view of the location for the digital camera and the selected target reference surface	30
Figure 3.2	A Canon EOS 400D digital SLR camera with 10.1 megapixels CMOS sensor of size, 22.2 mm x 14.8 mm.	33
Figure 3.3	A Nikon D200 prosumer digital SLR camera with 10.2 megapixels CCD sensor of size, 23.6 mm x 15.8 mm.	34
Figure 3.4	The front view of a Canon IXUS 40 consumer compact digital camera with 4.2 megapixels CCD sensor (sensor size, 5.75 mm x 4.31 mm).	35
Figure 3.5	The rear view of a Canon IXUS 40 consumer compact digital camera with position of the macro/infinity button shown.	35
Figure 3.6	A Bosch Auto Dome 300 series PTZ surveillance camera of 0.4 mega pixel (PAL) Charge-Couple-Device CCD.	36
Figure 3.7	Logitech Quick Cam Pro 4000 webcam.	37
Figure 3.8	Photograph noise at three different ISO setting for digital camera. (From website: http://www.zavosphotography.com /tips-and-techniques/a-beginners-guide-to-photography-part -1-intro-and-iso)	37
Figure 3.9	Schematic diagram of the experiment set-up to determine wavelengths of monochromatic light generated from the H-20 monochromator and the spectral sensitivity of a digital camera sensor.	40

Figure 3.10	A typical spectral sensitivity graphs to obtain the spectral bands of a digital camera sensor. (The Colour Group, 2016)	41
Figure 3.11	The flow chart for the method used to determine the spectral sensitivity and spectral bands for the digital camera sensors. (Adapted from Sigernes et al., 2008)	42
Figure 3.12	Schematic diagram of the experiment set-up to determine relationship between the irradiance and the digital numbers of images.	43
Figure 3.13	The flow chart for the method used to determine the relationship between the irradiance and the digital numbers of the images.	45
Figure 3.14	Graph of the long-term trend of visibility and its characterizations in the Pearl River Delta region (Deng et al. 2008).	47
Figure 3.15	The photograph showing the selected target reference surface as captured from the rooftop of School of Physics, Universiti Sains Malaysia at 11.30am on 15 May 2015.	48
Figure 3.16	The developed flow chart of the method used to develop the algorithm to determine the relationship between atmospheric aerosols concentration with the reflectance of the atmospheric aerosols.	49
Figure 3.17	The flow chart to determine the atmospheric aerosols concentration by the digital camera	52
Figure 4.1	The spectrum of monochromatic light generated by H-20 monochromator set at the wavelength of 425 nm. This spectrum was recorded by the ASD FieldSpec® HandHeld spectroradiometer.	54
Figure 4.2	The zoomed spectrum of monochromatic light set at the wavelength of 425 nm, showing the FWHM and the peak wavelength of spectrum.	56
Figure 4.3	Graph of the spectra of monochromatic light at different effective wavelengths (λeff) and uncertainty from H-20 monochromator set at wavelengths of 400 nm, 425 nm, 450 nm, 475 nm, 500 nm, 525 nm, 550 nm, 575 nm, 600 nm, 625 nm, 650 nm, 675 nm and 700 nm, reflected by a Lambertian screen.	57
Figure 4.4	The photograph of the monochromatic light at the λ_{eff} of (427 ± 4) nm which was reflected by a Lambertian screen captured by a Canon 400D DSLR camera. (Camera setting with ISO1600, aperture: F2.8 and exposure time: 6s).	59
Figure 4.5	The photographs of the Lambertian screen illuminated by the different λeff of monochromatic light were captured by a Canon 400D DSLR camera. (Camera setting ISO1600, aperture: F2.8, exposure time: 6s).	60
Figure 4.6	The RGB relative spectral sensitivity and the RGB spectral bands with standard deviation for Canon 400D DSLR camera sensor	61

Figure 4.7	The photographs of the Lambertian screen illuminated by the different λeff of monochromatic light were captured by a Nikon D200 DSLR camera. (Camera setting ISO1600, aperture: F2.8, exposure time: 6s).	62
Figure 4.8	The RGB relative spectral sensitivity and the RGB spectral bands with standard deviation for Nikon D200 DSLR camera sensor.	62
Figure 4.9	The photographs of the Lambertian screen illuminated by the different λ_{eff} of monochromatic light were captured by a Canon IXUS 40 camera. (Camera setting: Auto mode).	63
Figure 4.10	The RGB relative spectral sensitivity and the RGB spectral bands with standard deviation for Canon IXUS 40 compact camera sensor	63
Figure 4.11	The photographs of the Lambertian screen illuminated by the different λ_{eff} of monochromatic light were captured by a Logitech QuickCam Pro 4000 Webcam. (Camera setting: Auto mode).	64
Figure 4.12	The RGB relative spectral sensitivity and the RGB spectral bands with standard deviation for Logitech QuickCam Pro 4000 Webcam sensor.	64
Figure 4.13	The photographs of the Lambertian screen illuminated by the different λ_{eff} of monochromatic light were captured by a Bosch surveillance camera. (Camera setting: Auto mode).	65
Figure 4.14	The RGB relative spectral sensitivity and the RGB spectral bands with standard deviation for Bosch Auto Dome 300 Series surveillance camera sensor.	65
Figure 4.15	The spectral irradiance of the filtered light captured by the Canon 400D DSLR camera.	67
Figure 4.16	The isolated (i) red band, (ii) green band and (iii) blue band of the spectral irradiance of the colored filtered light captured by the Canon 400D DSLR camera.	68
Figure 4.17	The graphs of DN versus L for (i) red band, (ii) green band and (iii) blue band as captured by the Canon 400D DSLR camera.	70
Figure 4.18	The graph of average reflectance versus wavelength of the twenty four different batches of leaves from the target reference surface (100m – 200m above sea level).	74
Figure 4.19	The graph of average reflectance versus wavelength of the twenty four different batches of leaves from the target reference surface (200m – 300m above sea level).	74
Figure 4.20	The graph of average reflectance of the two regions versus wavelength of the twenty four batches of leaves from the target reference surface.	75

Figure 4.21	The average RGB digital numbers within the area of target reference surface of the photograph shown in Figure 3.15. (i) Red band, (ii) Green band and (iii) Blue band.	77
Figure 4.22	The spectral irradiance of diffused sunlight from the sky measured by ASD handheld spectroradiometer at the rooftop of the building for School of Physics at 11.30am on 15 May 2015.	78
Figure 4.23	The photograph captured by Canon 400D digital camera at 11.30am on 15 May 2015 which was used to determine the atmospheric aerosols concentration, P to be 55.7 $\mu g\ m^{-3}$.	87
Figure 4.24	The photograph captured by Nikon D200 digital camera at 11.00am on 15 May 2015 which was used to determine the atmospheric aerosols concentration, P to be 56.2 $\mu g\ m^{-3}$.	88
Figure 4.25	The photograph captured by Canon IXUS 40 digital camera at 3.30pm on 15 July 2011 which was used to determine the atmospheric aerosols concentration, P to be 55.6 $\mu g\ m^{-3}$.	88
Figure 4.26	The photograph captured by BOSCH auto dome 300 series surveillance digital camera at 8.46am on 1 April 2009 which was used to determine the atmospheric aerosols concentration, P to be 54.3$\mu g\ m^{-3}$.	89
Figure 4.27	The photograph captured by Logitech QuickCam Pro 4000 Webcam at 11.00am on 1 February 2008 which was used to determine the atmospheric aerosols concentration, P to be 57.4 $\mu g\ m^{-3}$.	89
Figure 4.28	The photographs captured by Canon 400D DSLR camera (during the haze period from September to December 2015) which were used to determine the atmospheric aerosols concentration, P.	91
Figure 4.29	Validation scatter plot of the atmospheric aerosols concentrations determined by using Canon 400D DSLR camera against the DustTrak™ readings.	93
Figure 4.30	Validation scatter plot of the atmospheric aerosols concentrations determined by using Nikon 200D DSLR camera against the DustTrak™ readings.	94
Figure 4.31	Validation scatter plot of the atmospheric aerosols concentrations determined by using Canon IXUS 40 digital camera against the DustTrak™ readings.	94
Figure 4.32	Validation scatter plot of the atmospheric aerosols concentrations determined by using BOSCH auto dome series surveillance digital camera against the DustTrak™ readings.	95
Figure 4.33	Validation scatter plot of the atmospheric aerosols concentrations determined by using Logitech QuickCam 4000 Webcam against the DustTrak™ readings.	95

LIST OF SYMBOLS

D_a	Aerodynamic diameter
P	Atmospheric aerosol concentration (PM_{10})
μ_v	Cosine of viewing angle
μ_s	Cosine of solar zenith angle
DN	Digital number
L	Irradiance
τ_a	Optical thickness for aerosols
τ_m	Optical thickness for molecules
R_{Atm}	Reflectance of the atmospheric aerosols
R_m	Reflectance of the atmospheric molecules
R_a	Reflectance of the atmospheric particles
R_T	Reflectance of the target reference surface
R_S	Reflectance recorded by the digital camera
$P_a(\Theta)$	Scattering phase function for aerosols
$P_m(\Theta)$	Scattering phase function for molecules
σ	Absorption
s	Finite path
τ	Optical depth
ρ	Density of absorbers
τ_a	Optical depth for particle aerosols
τ_m	Optical depth for molecule aerosols

LIST OF ABBREVIATIONS

API	Air Pollution Index
AQHI	Air Quality Health Index
AQI	Air Quality Indices
AOT	Atmospheric Optical Thickness
BAM	Beta Attenuation Monitoring
CAI-Asia	Clean Air Initiative for Asian Cities
CCD	Charge Coupled Device
CMOS	Complementary Metal-Oxide Semiconductor
CO_2	Carbon dioxide
DSLR	Digital Single Lens Reflex
EEA	European Environment Agency
EPA	United States Environment Protection Agency
FDMS	Filter Dynamics Measurement System
FWHM	Full Width Half Maximum
HEI	Health Effect Institute
IPU	Indeks Pencemaran Udara
NO_x	Nitrogen oxides
PAL	Phase Alternating Line
PM	Particulate Matter
$PM_{2.5}$	Particulate Matter with aerodynamic diameter less than 2.5 μm
PM_{10}	Particulate Matter with aerodynamic diameter less than 10 μm
PSI	Pollutant Standards Index
PTZ	Pan Tilt Zoom
SEM	Scanning Electron Microscope
SLR	Single Lens Reflex
SO_2	Sulphur dioxide
TEOM	Tapered Element Oscillating Microbalance
USM	Universiti Sains Malaysia
VGA	Video Graphics Array
WHO	World Health Organization

PEMBANGUNAN PENGUKURAN AEROSOL TERESTRIAL DENGAN MENGGUNAKAN KAMERA DIGITAL

ABSTRAK

Partikel atmosfera dengan diameter kurang daripada 10 μm (PM_{10}) merupakan komponen utama pencemaran udara yang mengancam kesihatan manusia dan persekitaran. Taburan stesen pemantauan kualiti udara yang sedia ada sekarang tidak cukup luas liputannya bagi mewakili semua kawasan. Tambahan pula, orang ramai tidak mempunyai akses yang cepat atau secara langsung kepada maklumat kualiti udara bagi mengambil langkah berjaga-jaga terhadap dedahan yang lama kepada kepekatan partikel atmosfera yang tinggi. Tujuan kajian ini adalah untuk membangunkan suatu pengukuran aerosol terestial dengan menggunakan kamera digital bagi menentukan kepekatan $PM_{10.}$ Lima kamera digital yang berlainan jenis pengesan, dengan resolusi dan saiz yang berbeza digunakan sebagai pengesan penderiaan jauh dalam kajian ini. Fungsi respon radiometrik bagi kelima-lima pengesan kamera digital ditentukan dan digunakan untuk mengukur sinaran yang direkod dalam gambarfoto digital. Suatu algoritma baharu telah dibangunkan untuk menukar nilai-nilai pixel multispektra yang diperoleh daripada kelima-lima kamera digital yang berbeza kepada nilai-nilai kuantitatif bagi kepekatan $PM_{10.}$ Apabila kepekatan PM_{10} bertambah, kepantulan cahaya matahari tersebar yang berinteraksi dengan partikel atmosfera juga bertambah. Algoritma tersebut telah dibangunkan berasaskan analisis regresi pada kepekatan PM_{10} yang diukur dengan kepantulan cahaya matahari tersebar yang berinteraksi dengan partikel atmosfera. Nilai-nilai kepekatan PM_{10} yang diukur menggunakan algoritma yang dibangunkan telah disahkan dengan membuat korelasi bersama nilai-nilai kepekatan PM_{10} yang diukur oleh meter DustTrak™. Keputusan daripada kajian ini menunjukkan bahawa aplikasi

algoritma yang baharu dibangunkan kepada kamera digital masing-masing menghasilkan pekali korelasi (R^2) yang tinggi dan ralat punca min kuasa dua (RMS) yang rendah di antara nilai sukatan meter DustTrak™ dengan nilai-nilai anggaran pengukuran kepekatan PM_{10} oleh kamera-kamera digital. Kedua-dua kamera DSLR menunjukkan ketepatan yang tinggi dalam penentuan kepekatan PM_{10} di mana kamera DSLR CCD mempunyai nilai R^2 = 0.8304, RMS=16.0 dan kamera DSLR CMOS mempunyai R^2 = 0.8424, RMS=17.0. Kajian selanjutnya boleh direplikasi dengan menggunakan kamera telefon mudah alih yang berlainan jenis.

DEVELOPMENT OF A TERRESTRIAL AEROSOL MEASUREMENTS USING DIGITAL CAMERAS

ABSTRACT

Atmospheric aerosols with diameters less than 10 µm (PM_{10}) are a major component of air pollution that threatens our health and our environment. Currently, distribution of air quality monitoring stations does not provide enough coverage for all areas. In addition, the public does not have direct nor immediate access to air quality information in order to take precaution against long exposure to high concentrations of atmospheric aerosols. The aim of this study is to develop a terrestrial aerosol measurement using the digital camera to determine the concentration of PM_{10}. Five digital cameras with different sensor types, sensor resolutions and sensor sizes were used as the remote sensing sensors in this study. The radiometric response function for these five digital camera sensors have been determined and used to measure the irradiance recorded in digital photographs. A newly developed algorithm was used to convert the multispectral pixel values acquired from the five different digital cameras into quantitative values of PM_{10} concentration. As the PM_{10} concentration increases, the reflectance of the diffused sunlight which interacted with the atmospheric aerosols also increases. This algorithm was developed based on the regression analysis of the measured PM_{10} concentration and the reflectance of the diffused sunlight which interacted with the atmospheric aerosols. The measured PM_{10} concentration values from this algorithm had been validated by correlating it with the PM_{10} concentration values measured by a DustTrak™ meter. The results of this study showed that the newly developed algorithms applied to the respective digital cameras, produced a high correlation coefficient (R^2) and low root-mean-square error (RMS) between the DustTrak™ meter measurements and the estimated PM_{10} concentration measurements

by the digital cameras. Both the DSLR cameras have the highest accuracy in determining PM_{10} concentration whereby the CCD DSLR camera has the value of R^2 = 0.8304, RMS = 16.0 and the CMOS DSLR camera has the value of R^2 = 0.8424, RMS = 17.0. Future work can be replicated by using different types of mobile phone cameras.

CHAPTER 1

INTRODUCTION

1.1 Background

In the last few decades, the air quality has profoundly deteriorated all over the world with the rapid growth of industrialization and urbanization (Duque et al., 2016; Martinelli et al., 2013; Silva et al., 2013; Banerjee and Srivatava, 2011; Chan et al., 2008; Fenger, 1999). Most pollutants in many urbanized areas are generated from the fossil fuel combustion in power stations and motor vehicles (European Environment Agency, 2013; Martinelli et al., 2013; Chan et al., 2008). Therefore, air quality in these areas has been affected over time due to the increase of fossil fuel consumption for economic development (Chan et al., 2008). For example, Figure 1.1 shows air pollutants being released from the Sultan Azlan Shah Coal Power Station in Manjung, Perak, Malaysia.

Figure 1.1: Air pollutants being released from the Sultan Azlan Shah Coal Power Station in Manjung, Perak, Malaysia. (Tenaga Nasional Berhad, 2014).

As reported by the European Environment Agency in year 2013, fossil fuel combustion releases air pollutants like sulphur dioxide (SO_2), fine particulate matter with the aerodynamic diameter less than 10 μm (PM_{10}), nitrogen oxides (NO_x), carbon dioxide (CO_2), mercury and other harmful substances into the air (European Environment Agency, 2013; Martinelli et al., 2013, Chan et al., 2008).

In year 2014, the Asian Green City Index reported the benchmarking data of the air quality for PM_{10}, SO_2 and NO_2 concentrations in 22 Asian cities (Asian Green City Index, 2014). This was the research project carried out by the Economist Intelligence Unit which was sponsored by Siemens. This report measures and rates the environmental performance of 22 Asian cities, which are capital cities as well as certain leading business centres selected for their size and importance.

Figure 1.2 shows a histogram which was constructed from the benchmarking data of the air quality reported in the Asian Green City Index, 2014. It clearly shows that in all of these 22 selected Asian cities, the annual average concentration of only PM_{10} greatly exceeded the current World Health Organization (WHO) health-based Air Quality Guidelines of 20 $\mu g/m^3$ (WHO, 2005). The histogram also shows that PM_{10}'s annual average concentration is the highest among all other air pollutants in all these 22 selected Asian cities

[Average air quality concentration of 22 Asian cities for PM_{10} = 107.8 µg/m^3, SO_2 = 22.5 µg/m^3 and NO_2 = 42.7 µg/m^3].

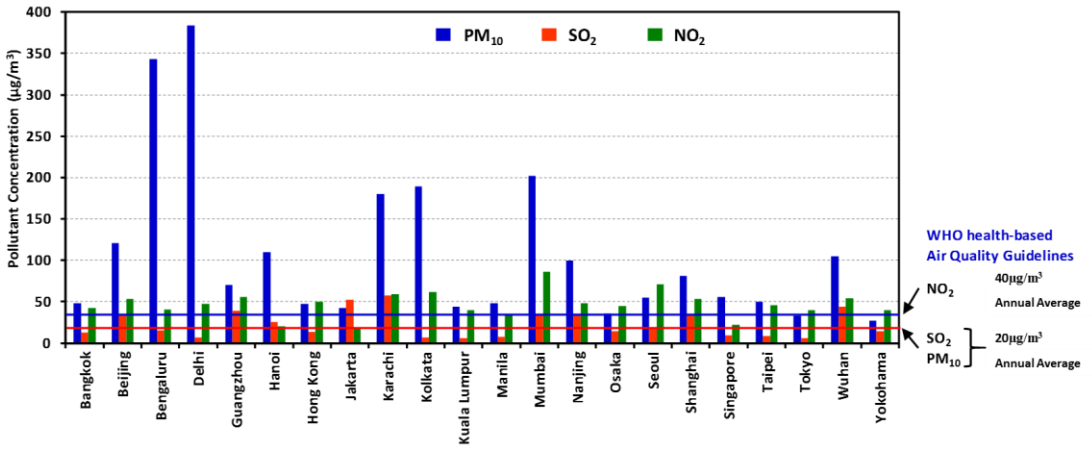

Figure 1.2: The annual average benchmarking data of the air quality for PM_{10}, SO_2, and NO_2 concentrations in twenty two selected Asian cities. (Asian Green City Index, 2014)

Figure 1.3 shows the Scanning Electron Microscope (SEM) images for soot particles of air pollutants from a coal-fired power plant in the report of United States Environmental Protection Agency, EPA (Cheng, 1979). Generally, the size of atmospheric aerosols is within the range of aerodynamic diameters from 0.001 µm to 100 µm (Seinfeld et al., 2006; Hinds, 1999; Cheng, 1979). These atmospheric aerosols are too small for our naked eye to see.

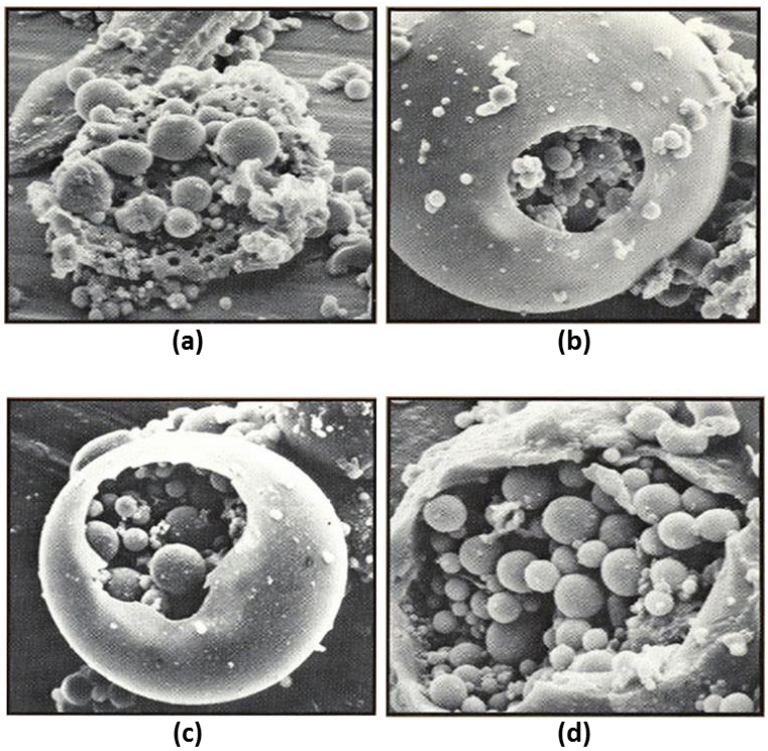

Figure 1.3: Images of Scanning Electron Microscope (SEM) for soot particles of air pollutants from a coal-fired power plant. Magnification: (a) 500X, (b) 1,500X, (c) 2,000X and (d) 2,500X (Cheng, 1979).

These microscopic atmospheric aerosols can be inhaled and embedded deeply in the lungs to cause serious health effects such as respiratory disease, cancer and other potentially deadly illnesses. Many scientific studies have gathered evidence to indicate that the most harmful component in air pollution is the microscopic atmospheric aerosols, particularly coarse aerosols, PM_{10} and fine aerosols, $PM_{2.5}$ (Donaldson et al., 2000; Pope et al., 2015, 2008, 2007, 2004, 1995), thus both the United Nations and WHO have declared that atmospheric aerosols is the greatest global threat. Therefore, more focused and prompt action should be taken to reduce air quality deterioration and to monitor closely the concentration of PM_{10} or atmospheric aerosols.

There are several method available for monitoring PM_{10} mass concentration. One method is the light scattering systems. It provides information on the number of particles present in different size ranges. They are based on the principle that there is a relationship between the scattering of light that reaches a particle and the particle size (Grimm and Eatough, 2009). This method was used to measure PM_{10} mass concentration in poultry and pig houses in comparison with gravimetric samplers (Cambra-López et al., 2015). A study to develop an instrument to measure PM_{10} concentration was reported using light scattering method (Morpurgo et al., 2012).

The next method is known as the Tapered Element Oscillating Microbalance (TEOM). In this method, sampled ambient air is allowed to pass at a constant flow rate through a filter, attached to a vibrating hollow tapered element. As PM_{10} is collected on the filter, the frequency of vibration of the element decreases. The mass of PM_{10} collected over a period of 15 min or one h can thus be calculated. The TEOM can be used for continuous, on-line monitoring. It uses a heated sample inlet to prevent moisture from contaminating the filter. PM_{10} concentration monitoring in Europe also used TEOM in compliance with the European Air Quality Standard (Muir, 2000). The implications of the TEOM software configuration on PM_{10} concentration measurements in the UK and Europe was also reported (Green et al., 2006). The TEOM was also used to compare with a newly developed PM_{10} concentration measuring instrument at the Institute of Occupational Medicine

(IOM), Edinburgh (Soutar et al., 1999). A study was carried out in the urban area of Genoa, Italy to measure the concentration of PM_{10}, $PM_{2.5}$, PM_1 by using the continuous monitor TEOM and the sequential sampler PARTISOL (Ariola et al., 2006). Based on the TEOM technology, the Filter Dynamics Measurement System (FDMS) which is a self-referencing airborne particulate monitor was developed to measure both core and volatile fractions of particles.

Beta Attenuation Monitors (BAM) are devices that draw sampled air at a constant flowrate through a section of paper tape, on which particles from the air are collected. Sampling period is between one to 24 h. Throughout this period transmission of beta particles through the tape (from a source inside the instrument) is measured. The concentration of PM_{10} is determine by the difference between the two measurements caused by the particulate matter collected in the tape. BAM can be used for continuous, on-line monitoring. This method was used to measure PM_{10} concentration at a North Las Vegas, Nevada sampling site (Watson et al., 2012). An assessment of factors influencing PM_{10} mass concentration measured by gravimetric and beta attenuation techniques was conducted at a suburban site in Athens, Greece, over a period of 4 years from 2009 to 2012 (Triantafyllou et al., 2016). A paper which discusses the repercussions of using Beta Attenuation Monitoring (BAM) detectors on the accuracy and reliability of Chile's National Air Quality Information System for measuring particulate matter was also reported (Toro A. et al., 2015).

The Filter-based gravimetric method (sampler PARTISOL) involves drawing a measured volume of air through a filter, which is weighed before and after the sampling period such as 24 h. The European reference sampler is a filter-based gravimetric method. This method cannot be used for continuous or on-line measurement because the filters must be weighed before and after exposure. This gravimetric method is required in Europe as well as in US for compliance measurements (Gehrig et al., 2005). It was used as the reference in a comparative field test for the measurement of PM_{10} dust in atmospheric air using the beta-absorption method in Gdańsk region, Poland between 1 January 2010 to 31 December 2010 (Gębicki and Szymańska, 2012). This manual gravimetric reference method was also used for a new method developed in Switzerland to link PM_{10} concentrations from automatic monitors (Gehrig et al., 2005).

1.2 Problem Statement

Air quality monitoring stations have been established in many major cities. For additional coverage, more stations would have to be built to alert the public regarding air quality. The public do not have direct access to this information and the released information may be too late to prevent one from being overexposed to the harmful PM_{10}. Since air quality also varies from place to place, measuring stations which are localised do not provide sufficient data for monitoring air pollution. Furthermore, ground stations are limited in

number due to high cost of instruments and facility maintenance (Tsai et al., 2011). Exposure to PM_{10} is highly personalized, dependent on how and where an individual lives, travels, works, and other activities (O'Neill et al., 2003). Only few studies have been done on personal monitors and they emphasize on indoor air quality (Williams et al., 2000).

1.3 Aim

The study aimed to develop a terrestrial aerosol measurement using the digital camera to determine the concentration of PM_{10}.

1.4 Objectives

The objectives of this study are as follows.

i) To determine the radiometric response function for five different digital camera sensors to measure irradiance captured in digital photographs.

ii) To develop the appropriate algorithms for measuring the atmospheric aerosols concentration (PM_{10}) from the images of target reference surface areas captured in the photographs by the five different digital cameras.

iii) To determine and validate the measurements of atmospheric aerosols concentration by using the digital camera.

1.5 Novelty and Significance

The novelty of this study is the development of the algorithm which can transform the image captured by the digital camera into the mass concentration of PM_{10}. In addition, the technique applied to capture the image is along the horizontal plane compared to the traditional top down vertical plane image capture. The significance of this study is the monitoring of in situ air quality using a commercial digital camera at any time of the day without a transporting vehicle.

1.6 Scope

In this study, the digital cameras used are limited to sensor types of charge-coupled device (CCD), video graphics array CCD (VGA CCD) and complementary metal-oxide-semiconductor (CMOS) only. The sensor resolution is between 0.3 to 10.2 Megapixels. The size of the sensors range from 4.60 mm x 3.97 mm to 23.6 mm x 15.8 mm. Three digital cameras were manually operated to capture the photographs whereas another two video digital cameras captured video images. All the photographs or images were taken from an elevated level on the rooftop of the School of Physics, USM main campus, Penang. The target reference surface area must be dark. Live green plants appear relatively dark in sunlight (Matevski et al., 2011). So the green vegetation of a distant hill at 2 km away from the camera was chosen as the target reference surface. The choice of this particular distance has been based

on the study by Deng et al., 2008, which reported that when the concentration of atmospheric aerosols reaches 400 μg m^{-3}, the visibility is limited to approximately 3 km. Hence the target distance of 2 km away would definitely be visible in order that for the image to be captured to determine the atmospheric aerosols concentration of 400 μg m^{-3} or less. According to the air pollution index released by the WHO (WHO, 2005) atmospheric aerosols concentration of more than 300 μg m^{-3} would be hazardous to public health. The monitoring time was from 8.30 am to 5.30 pm on ordinary and hazy days when there was enough day light for the image to be captured. No data was collected on cloudy or rainy days. An ASD FieldSpec® HandHeld spectroradiometer was used to measure the irradiance and reflectance of the green vegetation in this study. The DustTrak™ meter was used to measure atmospheric aerosols (PM_{10}) concentration in μg/m^{-3}. It was positioned beside the digital cameras. The DustTrak™ measurement was taken as soon as the digital cameras captured the photographs with the assumption that the PM_{10} concentration was homogeneous throughout the 2 km from the camera to the reference target. The 50 W halogen ASD Pro Lamp and the H-20 monochromator were used as the light sources for calibrating the digital cameras.

1.7 Thesis Overview

This thesis is divided into five chapters which are as follows:-

Chapter 1 begins with background of this study. It elaborates on the presence of atmospheric aerosols and their effect on health. A description of the different techniques to measure atmospheric aerosols concentration is presented. The problem statement, the aim, the objectives, the novelty and significance followed by the scope of this research are outlined. The thesis overview is also presented in this chapter.

Chapter 2 consists of literature reviews, the theory on atmospheric aerosols and researches that have been done including other techniques to measure atmospheric aerosols concentrations. The algorithm for determining atmospheric aerosols concentration was derived from the theory of atmospheric optical effects which was caused by the interaction between the diffused sunlight from the sky with the atmospheric aerosols and the target reference surface.

Chapter 3 describes the methodology applied in this study. It begins with the selection of digital cameras for this study, the digital cameras' settings for landscape photography, followed by the procedure on how to calibrate these digital cameras. The procedure and techniques to develop the algorithm for measuring the atmospheric aerosols concentration from the images of

target reference surface areas captured in the photographs are elaborated. A description of the method to determine the atmospheric aerosols concentration by applying the developed algorithm and the validation of the measurements are outlined.

Chapter 4 reports the results and discussion of the research data in this study. This includes the determination of spectral sensitivities and RGB spectral bands which were used to determine the radiometric response function for the five digital camera sensors. These radiometric response functions were used to measure the irradiance recorded in digital photographs and it was used to determine the reflectance from atmospheric aerosols. This is followed by the presentation of the algorithm development, the application of the newly developed algorithms to determine the atmospheric aerosols concentrations and the validation of these measurements in comparison with the readings of the DustTrak™ meter.

Finally, Chapter 5 describes the conclusion of this project. Some suggestions for future studies are also given in this chapter.

CHAPTER 2

LITERATURE REVIEW

2.1 Measurement of Atmospheric Aerosols

With the rapid growth of industrialization and urbanization, air pollution poses as a threat to the environment (Kim Oanh et al., 2006; Wu et al., 2006). In addition to this, air pollution also endangers our health (Pope et al., 2015; 2008; 2007; Banauch et al., 2006; Brunekreef and Holgate, 2002).

In order to understand how the atmosphere modifies remotely sensed data, atmospheric models can be used to help calculate the atmospheric attenuation in the region of visible and infrared light. LaRocca and Turner (1975) has compiled a detailed description of methods of calculating atmospheric transmittance and radiance. The turbid atmosphere is divided into three components namely the molecular or Rayleigh component, the aerosol-scattering component, and the ozone-absorption component for the purpose of a model. Two models have been derived based on the 1962 version of the U. S. Standard Atmosphere. The first model is characteristic of an atmosphere for which the meteorological range, or visibility, is 25 km at sea level (Elterman, 1964). The second model is for eight different meteorological ranges at sea level varying from 2 km to 13 km (Elterman, 1970).

Satellite images (Hadjimitsis, 2009; Lim et al., 2009; Hadjimitsis, 2008; Sifakis and Deschamps, 1992; Kaufman and Fraser, 1983), Atmospheric Optical Thickness (AOT) technique and other different techniques have been developed by many researchers to monitor the atmospheric aerosols concentration. The main drawback of satellite images is the disturbance of clouds especially in the equatorial region. Instead, the aerial photographic imagery technique is able to resolve the cloud problem to obtain air pollution map. These two techniques are costly and incur a delay in obtaining the measurement. However these two techniques uses the fundamental optical theory like light absorption, propagation, light scattering and light reflection. This technique has long been used for visibility monitoring (Diederen et al., 1985; Horvath and Noll, 1969; Middleton, 1968; Noll et al., 1968) using photographic film.

Light-attenuating gases and particles in the atmosphere will affect visibility (Singh et al., 2008; Sequeira and Lai, 1998). One of the effective air quality monitoring methods is the measurement of visibility. In general, visibility has been measured optically (Shen et al., 2014; Werner et al., 2005; Appel et al., 1985; Groblicki et al., 1981; Chan et al., 1999). Two kinds of optical method are used to measure visibility. One of them is to quantify an amount of photon that is transmitted through an ambient air from a light source in a transmitter unit to a detector in a receiver unit. Another method is to detect the forward or backward scattered light by the airborne particles using an

optical sensor in a receiver. The optical methods for visibility measurement produce a light extinction coefficient or a light scattering coefficient (Moosmüller et al., 2005; Lai and Sequeira 2001). These coefficients can be converted to visual range using Koschmieder's equation (Koschmieder, 1924). Visibility has been denoted as visual range for meteorological purposes (Ozkaynak et al., 1985).

The definition of visibility is the longest distance at which a black object can be observed against the horizon. Theoretically, visual range derived from light attenuation by gases and particles which exist between a light source and a detector in the atmosphere are produced by optical measurements. The distance to install these devices are within several tens of centimeters to several kilometers (Li and Sun, 2009; Gebhart et al., 2001; Johnson, 1981). It should be assumed that the distribution of gases and particles is homogeneous in the atmosphere in order to apply the visual range data to surrounded ambient air.

When an observer looks at distant regions or different directions from an instrument site, the optical based visual range derived from atmospheric light extinction may produce a certain uncertainty. So, the optical measurement value has spatial limitation.

Camera-based visibility monitoring techniques have been used to determine visual range (Liaw et al., 2009; Xie et al., 2008; Nagata et al., 2008). Studies on visibility measurement technique often used digital images. This technique required the detection of a man-made target or separate additional equipment (Bäumer et al., 2008). Visibility was classified into several levels or estimated from the distance at which a selected target can be seen using a contrast in an image. Some of the methods were applied to shorter distances on roads for fog detection (Babari et al., 2012). Luo et al. (2005) estimated visibility using a Sobel operator and fast Fourier transform in the frequency domain. However, they did not use optical-based monitoring for data comparison. For a landscape feature, a contrast in an image domain was also used to estimate atmospheric light extinction. Hautiére et al. (2011) proposed a probabilistic model-based approach which takes into consideration the distribution of contrasts in the scene. Digital image analysis schemes based on high-pass filters was introduced. And the colour difference analysis (Kim and Kim, 2005) was adopted to estimate visual range using the correlation between the colour difference and the light extinction coefficient.

In the last decade, there has been a tremendous leap in the advancement of digital photography technology. Today digital cameras have become more sophisticated to produce better images; they are easily portable, affordable and widely owned. This study gears to develop an alternative technique utilizing the availability of digital cameras to record measurement of atmospheric aerosols concentration anywhere, anyone and any time.

2.2 Atmospheric Aerosols

Atmospheric aerosols are a mixture of solid and liquid tiny particles suspended in the atmosphere (Seinfeld and Pandis, 2006; Hinds, 1999), which is also known as particulate matter (PM), fine particles and soot. These particles may be produced by natural processes, such as soil erosion, dust storms, volcanoes, wildfires, ocean salt spray and pollen. Apart from that, human activities such as fossil fuel combustion, use of motor vehicles, rock crushing, cement production, agricultural operations and wood burning also generate significant amounts of particles. The concentration, composition, and size distribution of atmospheric aerosol particles are highly variable in different places. In the lower atmosphere (troposphere) the total particle number and mass concentrations typically vary in the range of about 10^2–10^5 cm^{-3} and 1–100 $\mu g\ m^{-3}$, respectively (Pöschl, 2005).

2.2.1 Size and Behaviour of Atmospheric Aerosols

The behaviour of atmospheric aerosols is mainly determined by its size. As these atmospheric aerosols are not necessarily spherical in shape but instead are in irregular shapes, thus diameter cannot be used to express its actual or physical size. Normally the size of this atmospheric aerosol is expressed in terms of the aerodynamic diameter, D_a. The definition of aerodynamic diameter is as illustrated in Figure 2.1. Consider two particles X and Y. Particle X is spherical in shape while particle Y is irregular in shape,

both having a density of 1 g cm^{-3} (unit density). The irregularly shape particle Y and spherical particle X are defined to have the same aerodynamic diameter, D_a, if both their gravitational setting velocity, V_s, in air are the same, regardless of the particle Y's size, shape or density.

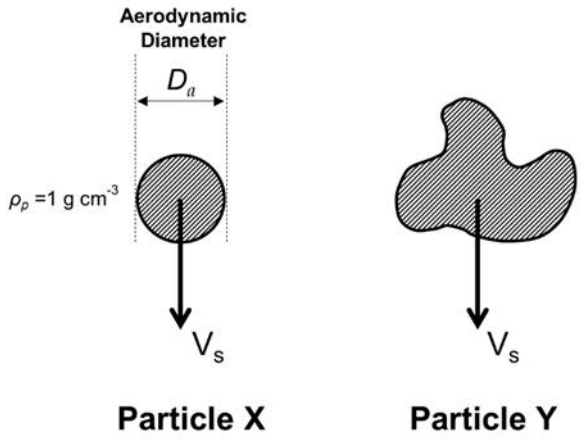

Figure 2.1: An illustration of the definition of aerodynamic diameter, D_a for two particles of different shapes (Hinds, 1999).

Generally, the size of atmospheric aerosols is within the range of aerodynamic diameters from 0.001 μm to 100 μm (Seinfeld and Pandis, 2006; Hinds, 1999). These atmospheric aerosols are too small for our naked eye to see. The morphological characteristics of atmospheric aerosols in the atmosphere can be categorized into three types of aerosols according to their size, which is super-coarse aerosols, coarse aerosols and fine aerosols. The atmospheric aerosols with aerodynamic diameter greater than 50 μm is known as super-coarse aerosols, which are heavier compared to the other two types of aerosols. Therefore it only remains in the air for a few minutes and then

settles near its source. The coarse aerosols or PM_{10}, is the atmospheric aerosols with the aerodynamic diameter less than 10 μm. These coarse aerosols are lighter than super-coarse aerosols. Thus PM_{10} can remain in the air for several days. As a result, it can be blown and spread by winds over a wide range of areas or for long distances from their original source. Atmospheric aerosols with aerodynamic diameter less than 2.5 μm are known as fine aerosols or $PM_{2.5}$. These fine aerosols are the lightest among the three types of aerosols. Thus it may remain in the atmosphere indefinitely as well as be widely spread.

2.2.2 The Level of Air Pollution for Atmospheric Aerosols

In general, the smaller and lighter an aerosol is, the longer it can stay in the atmosphere and can also travel a further distance away. Over time with the accumulation effects, more aerosols will remain in the atmosphere and the extent of air pollution will become more serious. In order to know the level of air pollution, many researchers measure the concentration of coarse (PM_{10}) and fine ($PM_{2.5}$) atmospheric aerosols as the indicator to describe the extent of air pollution. The definition of aerosols concentration is a measure of the amount of aerosol particles (e.g. number, mass, volume) in a unit volume of air. Normally the SI unit for aerosols mass concentration is expressed in $\mu g/m^3$.

Government agencies use air quality indices (AQI) as indicators of the ambient air quality. Normally the air pollutants taken into consideration to compute these air quality indices are the air pollutants that have adverse health effects and the environment, like particulate matter (PM_{10}), sulphur dioxide, nitrogen dioxide, carbon monoxide and ground-level ozone. In different countries, they use different air quality indices; for example Air Quality Index (AQI), Air Pollution Index (API), Air Quality Health Index (AQHI) and Pollutant Standards Index (PSI).

The indicator used in Malaysia to gauge the level of ambient air pollutants is Air Pollution Index (API) or "Indeks Pencemaran Udara" (IPU). The Malaysian government has associated this API with health classification, health effects and health advice, as shown in Table 2.1. When the API reading is 100 or below, the air pollutant level is in satisfactory condition and pose no acute or immediate health effects. Thus the public can have their usual outdoor activities. However, long term exposure to a moderate air pollution level (API consistently remaining at 51 to 100) for a period such as one year, might encounter chronic health effects.

The API reading above 100 means that air pollution level is in the unhealthy condition and this might affect public health. So, the precautionary action is to avoid unnecessary exposure to the polluted air. In other words, outdoor activities are not advisable.

Table 2.1: The official Health Implications of the respective Air Pollution Index (API) in Malaysia **(Source: Department of Environment, Ministry of Natural Resources and Environment, Malaysia)**.

API	Status	Health Effect	Health Advice
0 – 50	**Good**	Low pollution without any bad effect on health	No restriction for outdoor activities to the public. Maintain healthy lifestyle
51 – 100	**Moderate**	Moderate pollution that does not pose any bad effect on health	No restriction for outdoor activities to the public. Maintain healthy lifestyle
101 – 200	**Unhealthy**	Worsen the health condition of high risk people like people with heart and lung complications	Limited outdoor activities for the high risk people. Public need to reduce the extreme outdoor activities
201 – 300	**Very Unhealthy**	Worsen the health condition of people with heart and lung complications (low tolerance to outdoor physical exercises). Affect public health.	Old and high risk people are advised to stay indoors and reduce physical activities. People with health complications are advised to see the doctor.
> 300	**Hazardous**	Hazardous to high risk people and public health	Old and high risk people are prohibited for outdoor activities. Public are advised to abstain from outdoor activities
> 500	**Emergency**	Hazardous to high risk people and public health	Public are advised to follow orders from National Security Council and always follow the announcement in mass media

Numerous scientific studies have gathered evidence to indicate that the most harmful component in air pollution is the microscopic atmospheric aerosols, particularly coarse aerosols, PM_{10} and fine aerosols, $PM_{2.5}$ (Pope et al., 2015; 2008; 2007; 2004; 1995; Donaldson et al., 2000). In this thesis, the focus will be given to the atmospheric aerosols with the aerodynamic diameter less than 10 μm (PM_{10}), because monitoring of PM_{10} gives a bigger tolerance as it includes $PM_{2.5}$ as well.

With the ability of these microscopic aerosols to remain in the atmosphere indefinitely and due to accumulation effects, these aerosols have become a major global environmental issue. Other than damaging our environment continuously (Ramanathan and Feng, 2009; Ramanathan and Carmichael, 2008), this air pollution is also endangering our health (Pope et al., 2009; 2008; 2007; 2006; 2004; 2002; 1995; Banauch et al., 2006; Brunekreef and Holgate, 2002).

2.3 Visibility Related Atmospheric Aerosols Concentration

Our viewing of distance objects is affected by the presence of aerosols in the atmosphere. It has clearly showed in polluted air, the visual range reduce to less than a few kilometers. This phenomenon occurred because the atmospheric aerosols attenuate the light rays reflected by scene objects travel to the observer. Noll et al. (1968), Charlson et al. (1967) and Steffen (1956) reported that the atmospheric aerosol concentration is approximate proportional to the extinction coefficient due to light scattering. The degree of visibility degradation is based on the amount of aerosol concentration in the atmosphere. Noll et al. (1968) have reported this reciprocal relationship.

The images captured in outdoor scenes are usually degraded by the turbid medium in the atmosphere. Bad weather such as fog and haze reduce the visibility and color fidelity, and the particles in atmosphere cause absorption and scattering. The irradiance received by the camera from the scene point is

attenuated along the line of sight. Furthermore, the incoming light is blended with the airlight (He et al., 2011), which is ambient light reflected into the line of sight by atmospheric particles. The degraded images lose the contrast and color fidelity of the scene. In addition, the amount of degradation depends on the distances of the scene points from the camera.

2.4 Theoretical Derivation of Algorithm

In this study, a new algorithm has been developed to compute the real time PM_{10} concentration. In this part, this algorithm was developed based on the fundamental atmospheric optical theory (Appendix A) of light absorption and scattering (Slater, 1980; Hinds, 1999).

Figure 2.2 shows the aerial perspective model used in this study. The electromagnetic radiation from the sun in the sky (diffuse sunlight) towards the digital camera which is then recorded as the sensor reflectance, R_S. During the propagation towards the digital camera, the diffuse sunlight encountered two types of reflection; one being the reflection from a target reference surface and the other one being the reflection from the atmospheric aerosols. The assumption in this case is that there are no reflections contributed by other sources. The electromagnetic radiation reflected by the target reference surface is known as target reflectance, R_T. The electromagnetic radiation penetrating through the ambient pollutant column is reflected by the atmospheric aerosols

and is known as the atmospheric aerosols reflectance, R_{Atm}. This is the skylight parameter model which is applied in this project.

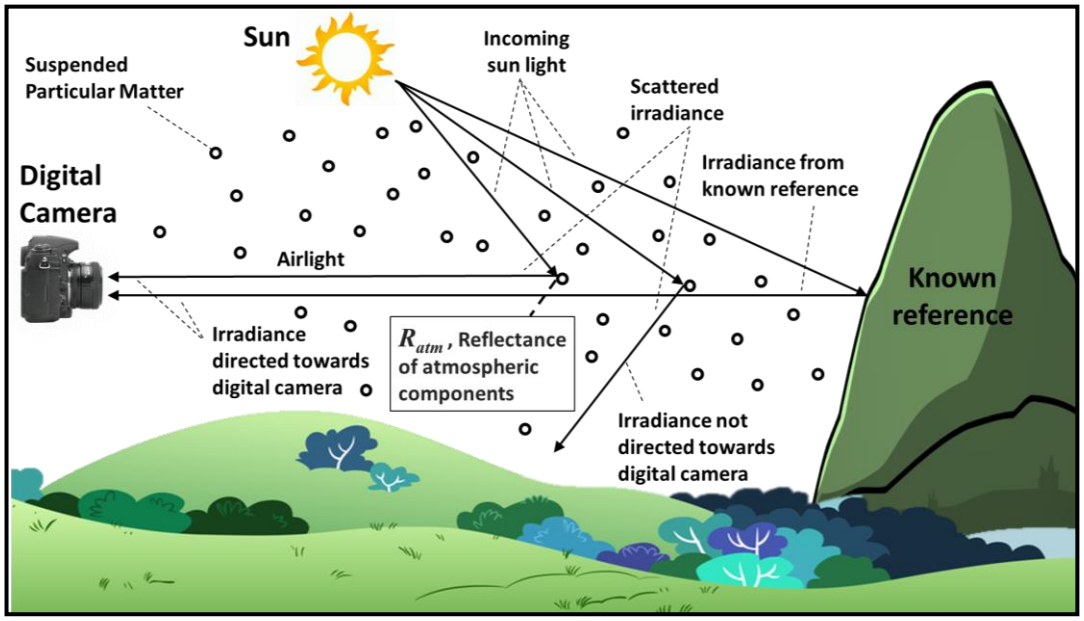

Figure 2.2: The aerial perspective model to show the digital camera recording the lights propagated through atmospheric the pollutant column. These lights are from reflected light of target reference surface, R_T and reflected light of atmospheric aerosols, R_{Atm}.

A new algorithm was developed to determine the atmospheric aerosols concentration using digital camera based on the theory that the more the atmospheric aerosols concentration, the more the reflectance from the atmospheric aerosols. The light received by the digital camera comes from the light reflected from the atmospheric aerosols as well as the reflected light from the target reference surface only; the assumption is that the other sources of light are not recorded by the camera. Reflectance is the ratio of the radiance reflected by the surface to the radiance received by the surface. So, the reflectance of atmospheric aerosols, R_{Atm} is given by the equation